Baggio, Mariangela; Hu, Yong; Tamminen, Aleksi; Nefedova, Irina; Ala-Laurinaho, Juha; Taylor, Zachary

Submillimeter-wave imaging assisted alignment of millimeter-wave spectroscopic system for quantification of corneal water content

Published in:
SPIE Conference Proceedings

DOI:
10.1117/12.2556309

Published: 01/01/2020

Document Version
Publisher's PDF, also known as Version of record

Please cite the original version:
Baggio, M., Hu, Y., Tamminen, A., Nefedova, I., Ala-Laurinaho, J., & Taylor, Z. (2020). Submillimeter-wave imaging assisted alignment of millimeter-wave spectroscopic system for quantification of corneal water content. In M. Jarrahi, S. Preu, & D. Turchinovich (Eds.), *SPIE Conference Proceedings* Article 113480M (Proceedings of SPIE : the International Society for Optical Engineering; Vol. 11348). SPIE. https://doi.org/10.1117/12.2556309

Submillimeter-wave imaging assisted alignment of millimeter-wave spectroscopic system for quantification of corneal water content

Baggio, Mariangela, Hu, Yong, Tamminen, Aleksi, Nefedova, Irina, Ala-Laurinaho, Juha, et al.

Mariangela Baggio, Yong Hu, Aleksi Tamminen, Irina Nefedova, Juha Ala-Laurinaho, Zachary Taylor, "Submillimeter-wave imaging assisted alignment of millimeter-wave spectroscopic system for quantification of corneal water content," Proc. SPIE 11348, Terahertz Photonics, 113480M (6 April 2020); doi: 10.1117/12.2556309

Event: SPIE Photonics Europe, 2020, Online Only, France

Submillimeter-wave imaging assisted alignment of millimeter-wave spectroscopic system for quantification of corneal water content

Mariangela Baggio[*a,b], Yong Hu[*c,], Aleksi Tamminen[a,b], Irina Nefedova[a,b], Juha Ala-Laurinaho[a,b], Zachary Taylor[a,b]
[a]Department of Electronics and Nanoengineering, Aalto University, Maarintie 8, Espoo, Finland
[b]Millilab, PO Box 1000 FI-02044 VTT, Finland
[c]Department of Head and Neck Surgery, University of California, Los Angeles, CA, USA 90025

ABSTRACT

We propose an alignment strategy for millimeter spectroscopy of cornea that uses imaging to screen for sufficient alignment conditions. The performance of different corneal imaging objectives, in the presence of misalignment, is evaluated. The cornea is illuminated with a TEM00 Gaussian beam at 650 GHz and the beam is swept across the cornea. Images are generated by calculating the coupling between illumination and scattered beams for each illumination beam position and angle. The cornea is displaced at intervals of 500 microns in the transverse and axial directions and with new coupling coefficient maps generated at each misaligned position. Contrast in the misaligned cases are compared to the aligned case via zero normalized spatial cross correlation. The results show a maximum normalized cross correlation of 0.92 for a two-mirror scanning system and 0.74 for a one-mirror scanning objective. The analysis suggests that imaging contrast at 650 GHz can be used to screen for misalignment that would be difficult to detect with MMW.

Keywords: Cornea, medical imaging, quasioptics, physical optics, THz, THz imaging, submillimeter wave remote sensing

1. INTRODUCTION

Millimeter and submillimeter-wave imaging of the cornea may offer valuable utility for corneal disease detection and monitoring. MMW and SUBMMW systems have sensitivity to water content due to large dispersive water permittivity at these bands[1]. Typical population variation in corneal geometry is on the order of free space submillimeter wavelengths[2]. Additionally, corneal tissue structure is exceptionally homogenous compared to other biological tissues[3]. These attributes suggest that MMW and SUBMMW frequencies can be used to analyze corneal tissue with minimal confounding effects from normal physiologic variation.

Perturbations in cornea thickness and water contents are associated with both eye diseases, such as Keratoconus and Fuchs' endothelial dystrophy, as well as corneal graft rejection after corneal surgeries as Penetrating Keratoplasty (PK), Deep Lamellar Endothelial Keratoplasty (DLEK), Descemet Stripping and Endothelium Keratoplasty (DSEK), and Descemet Membrane Endothelial Keratoplasty (DMEK). Currently, in a clinical setting corneal thickness is measured with established techniques, e.g. pachymetry or optical coherence tomography, however, there is no established or proven technique to measure *in vivo* cornea water content reliably.

Related results[3] indicate that the millimeter and submillimeter wave bands (~100 GHz – 400 GHz) are ideal for ascertaining corneal permittivity with measurements enhanced by the cornea's stratified media structure. The cornea and its proximity to the aqueous humor create a natural thin film that can be probed with wavelengths that are (1) sufficiently short to access, at the very least, the first resonant feature, and (2) sufficiently long to enable sufficient SNR. Resolution of the lossy standing waves across an ensemble of frequencies enables extraction of corneal permittivity. Numerous dielectric spectroscopic processing techniques can then be applied to further extract water content.

In an ophthalmic, patient imaging scenario, significant, time varying misalignment is frequent and is affected by erroneous positioning of the patients' eyes and head, involuntary movement of the head and body, and, to a lesser extent involuntary and rapid eye movements such as saccades. A common system strategy is to rapidly, and continuously acquire imaging data while monitoring some metric for image fidelity. This strategy often relies on qualitative assessments of image clarity; the medical professional keeps acquiring images until one of them "looks good". In submillimeter-wave spectroscopy of

Terahertz Photonics, edited by Mona Jarrahi, Sascha Preu, Dmitry Turchinovich, Proc. of SPIE
Vol. 11348, 113480M · © 2020 SPIE · CCC code: 0277-786X/20/$21 · doi: 10.1117/12.2556309

cornea, spectra can be acquired rapidly but the frequency dependent perturbations can obscure spectral signatures arising from the target parameters; corneal thickness and corneal water content.

In this work, we focus on an augmenting system that acquires quantitative measurements of central cornea hydration with a relatively large, stationary SUBMMW beam. Matching incoming submillimeter wave beam radius of curvature to that of the cornea (~ 7.5 mm – 8.0 mm) requires fast optics and a focused beam waist radius on the order of a wavelength. These parameters necessitate an electrically large collimated beam diameter prior to the final focusing optic and result in a large beam waist at the corneal surface thus limiting the utility of imaging based on beam scanning. Discussions with ophthalmology collaborators have identified many candidate diseases where there is no expected spatial variation in corneal water content across the surface thus a diagnostic system that does not image water content but instead senses aggregate water content is sufficient. Therefore, we consider a canonical, lens-coupled MMW spectroscopy system that can extract information about the cornea physiology (thickness, water content) but cannot deconvolve physiology related contrast from signal variation due to misalignment. We then consider a SUBMMW imaging system, compatible and integrated with the MMW system. The system operates at 650 GHz, is insensitive to corneal physiology, but has image contrast strongly dependent on the corneal position. This 650 GHz system can then be used to verify target alignment and identify MMW spectra that is of sufficient fidelity for cornea physiology extraction.

2. A SUBMILLIMETER-WAVE ADJUNCT, ALIGNMENT SYSTEM

Previous work at 650 GHz revealed substantial misalignment sensitivity where beam walk-off, due to imperfect alignment, resulted in signal detection levels with insufficient SNR for imaging. Deviations in corneal center of curvature (CoC) position as small as 1 mm produced SNRs less than 1. Conversely, systems operating at 100 GHz demonstrated limited return signal variation when displacement is within the ~ 1 - 2 mm range. These results suggest that an imaging system design that combines MMW and SUBMMW frequencies. If the beam paths for both bands is well-defined, the THz-frequency image can be used to validate alignment while the MMW data can be processed for the corneal permittivity and without the confounding effects of misalignment.

While the cornea presents as a lossy stratified medium at MMW frequencies, the precipitous absorption drop in penetration as a function of increasing frequencies renders high frequency radiation to surface level probing. The 2-pass absorption at 650 GHz illumination is > 20 dB and thus the cornea effectively presents as a half space. Thus, one can consider contrast at 650 GHz as a strong function of corneal geometry and placement error with respect to the aperture, and a weak function of the corneal physiology.

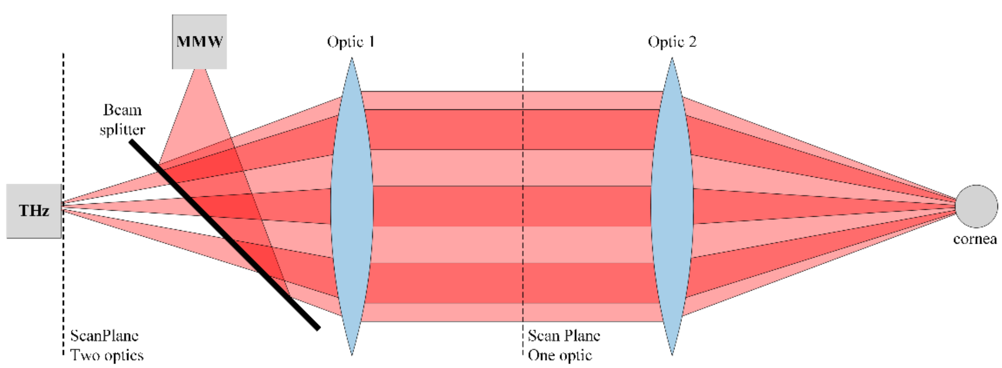

Figure 1: Proposed time-domain system model. Both imaging and the alignment use the same optics. It is also possible to use the same architecture in a frequency domain system

The increased frequency also allows for phase-front curvature matching with a smaller beam-waist radius on the cornea and thus a smaller collimated beam on target. Thus, it is possible to perform imaging at 650 GHz with the same optics used to illuminate the cornea at MMW. A schematic of this strategy is shown in Figure 1. A MMW subsystem and SUBMMW subsystem are optically collocated with a beam splitter. The MMW system provide a beam that fills the clear aperture of the first optic and is focused onto the cornea by the second optic. The scattered beam is redirected to the MMW subsystem. A SUBMMW subsystem provides an angularly-scanned, diverging beam. This scanned beam is collimated and focused to the cornea by the two optics. Scattered radiation is rerouted back the SUBMMW subsystem by the same optics.

In a patient imaging scenario, both the MMW spectroscopic data and SUBMMW imaging data are acquired continuously and simultaneously. The operator (or machine software) monitors the SUBMMW image and, when the observed contrast matches the known contrast of the aligned case, the system assures that the misalignment artifacts in the concomitantly acquired MMW data are minimized. Sections 5 and 6 introduce the zero-normalized cross correlation coefficient as an automated determination of alignment.

3. CANDIDATE OPTICS AND ANALYSIS OF IMAGING OBJECTIVES

We investigate imaging system designs employing a series of off-axis parabolic mirrors (OAP). OAP mirrors where chosen for their frequency invariant optical properties. A typical optical trail is comprised of three blocks: (1) a transceiver consisting of a source, detector, and optics that mate it with (2) a scanning system that modulates the beam f/#, and optical axis position/angle, and (3) a final objective which guides the beam to the cornea at normal incidence. The scanning optics can be realized by (1) moving two planar scanning mirrors or (2) by rotating a single galvanic mirror. In this paper, we will refer to them as (1) 1-mirror objective and (2) 2-mirror objective, respectively.

In order to understand the system behavior, we should be able to characterize the final block: the scanning objective, which is based on the chosen scanning optic method. The remaining part of the system can be designed to support this design or enhance some if its features. In both proposed designs, we aim to realize the same scanning of a hemispherical target, the cornea. The cornea center of curvature is placed at the focus position of a 90° off-axis parabolic mirror. The mirror effective focal length is 50.8 mm, while its aperture is 76.2 mm. The cornea can be scanned by illuminating the right location of the objective mirror surface. Since cornea is a spherical surface, a gaussian beam with a narrow beam waist hits it at normal incidence, so we can use the same optical trail for the target-to-detector path.

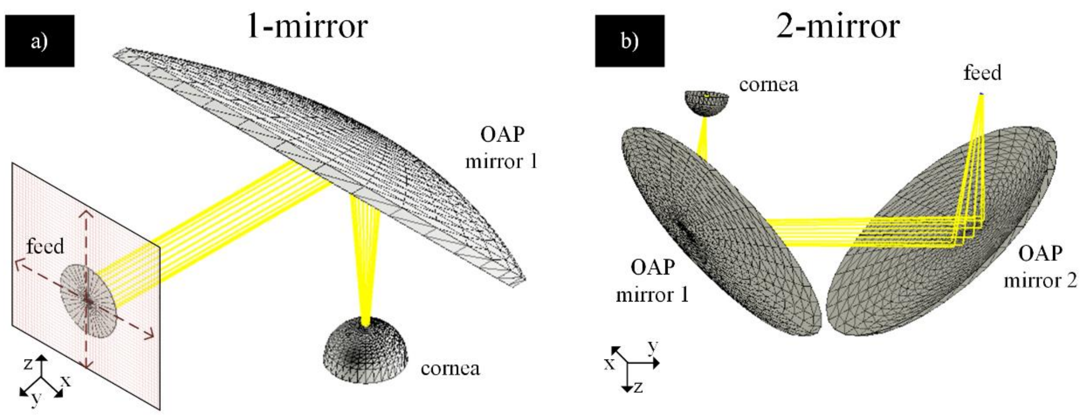

Figure 2: a) Objective optics of the 1-mirror objective. The scanning is realized by moving a gaussian beam feed on a transversal plane b) Objective optics of the 2-mirror objective. The scanning is realized by rotating a gaussian beam feed placed at the focus of an OAP mirror.

In the 1-mirror objective the spherical target is scanned by moving a collimated gaussian beam on a plane which moves on a transversal plane above the objective mirror. The scanning method is explained by Sung et al.[2]. In the 2-mirror objective the scanning is performed by rotating a gaussian beam feed in front of a second OAP mirror. The feed rotation angles correspond to the surface spherical coordinates on the cornea. Scanning, imaging objectives typically return a collected beam coaxial to the return beam and are retrodirective in nature. Therefore, as a first step, it is sufficient to consider the performance of the imaging objective as representative of full optical system behavior.

4. SIMULATION METHODS

Simulations were performed at 650 GHz through the physical optics method. Physical optics is valid when scatterers have dimensions of several wavelengths. The method can be performed sequentially from one scatterer surface to the next. The electromagnetic field is computed from a scalar Green function and the equivalent surface current densities induced by the incident electromagnetic field on each scatterer. More precisely, the electromagnetic field $(\vec{E}(\vec{r}),\ \vec{H}(\vec{r}))$ at the position in space $\vec{r}$,scattered by a surface A is computed with the formulas:

1

$$\vec{\mathrm{E}}(\vec{\mathrm{r}}) = -\oiint_A \nabla G(\vec{\mathrm{r}} - \vec{\mathrm{r}'}) \times \overrightarrow{\mathrm{J_{ms}}}(\vec{\mathrm{r}'}) dA \tag{2}$$

$$\vec{\mathrm{H}}(\vec{\mathrm{r}}) = \oiint_A \nabla G(\vec{\mathrm{r}} - \vec{\mathrm{r}'}) \times \vec{\mathrm{J}_s}(\vec{\mathrm{r}'}) dA, \tag{3}$$

$$\overrightarrow{\mathrm{J_{ms}}}(\vec{r'}) = -2\hat{\mathrm{n}} \times \vec{\mathrm{E}_\mathrm{I}}(\vec{\mathrm{r}'}) \tag{4}$$

$$\vec{\mathrm{J}_\mathrm{s}}(\vec{r'}) = 2\hat{\mathrm{n}} \times \vec{\mathrm{H}_\mathrm{I}}(\vec{\mathrm{r}'}) \tag{5}$$

where $\vec{r'}$ is the position on the scatterer surface A, $\vec{\mathrm{J}_\mathrm{s}}$ and , $\overrightarrow{\mathrm{J_{ms}}}$ are the equivalent electric and magnetic surface current densities, respectively, induced on the surface A by an incident electromagnetic field ($\vec{\mathrm{E}_\mathrm{I}}(\vec{\mathrm{r}'})$, $\vec{\mathrm{H}_\mathrm{I}}(\vec{\mathrm{r}'})$)

The test target was a perfect electric conductor (PEC) sphere of radius 8 mm. An example of illumination and scattered fields in the 1-mirror system is shown in Figure 3. The scattered electric field distribution has been distorted by the OAP. Even though OAPs are not affected by spherical aberrations, they are affected by astigmatism, coma and distortions and introduce cross-polarization in an incident electromagnetic field[4].

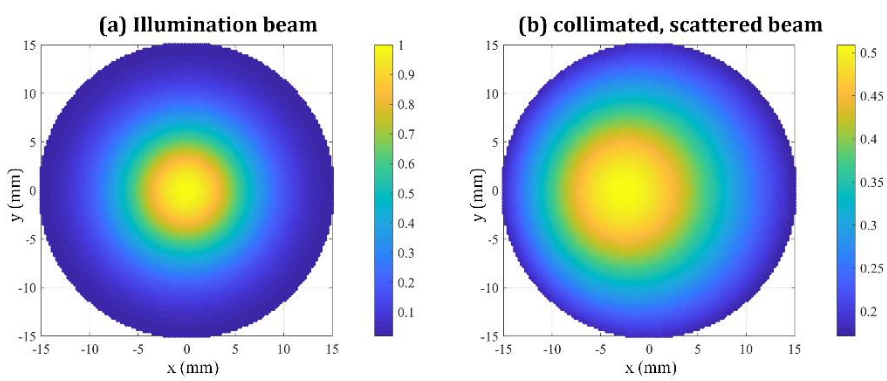

Figure 3: a) Normalized amplitude of the electric field E_i at the feed. The electric field has a gaussian distribution b) normalized amplitude of the electric field E_r reflected back in the same plane for the cornea apex location. It is noticeable how the beam waist shape has been distorted. The corresponding coupling coefficient is 0.66.

5. GENERATION OF COUPLING COEFFICIENT IMAGES AND NORMALIZED CROSS-CORRELATION MAPS

Alignment sensitivity was assessed over a 2 mm x 2 mm x 2mm cube of corneal positions centered at the focal point of the scanning objective, i.e. the scan range was ±1 mm about the focal point. Previous experimental work with parabolic mirror-based systems has indicated that displacements beyond one millimeter produce only little detectable signal. An ensemble of corneal positions on a plane coincident with the mirror focal point and normal to the optical axis are displayed in Figure 4a. This is labeled the “z = 0” plane. The CoC’s are indicated by the ‘o’ markers and the enface perimeter of each cornea is indicated by the black contours and grey transparent fill. The aligned case (optical axis pierces the CoC) is denoted with the green ‘o’ marker and green perimeter. This ensemble represents 25 different cornea positions positioned in a uniformly sampled rectilinear grid. The 3D grid of considered positions is displayed in Figure 5b. Five planes equally spaced at 0.5 mm along the optical axis are defined and 25 positions in each plane on a 0.5 mm grid are further defined. All grids are centered along the optical axis.

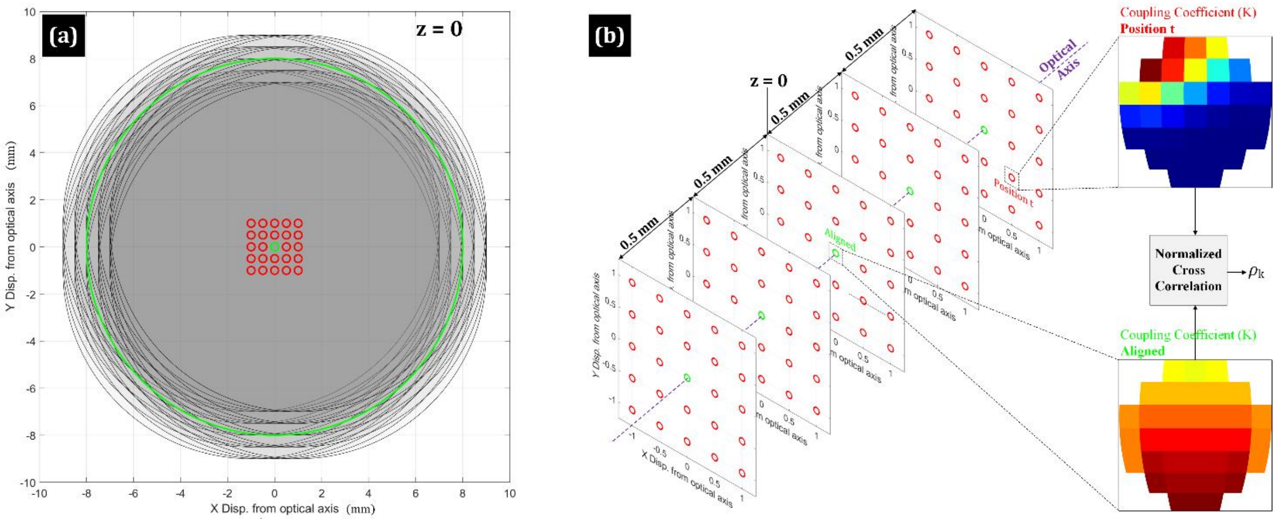

Figure 4: a)Spacing ensamble of cornea positions on a plane coincident to with the mirror focal point b) The normalized cross correlation is realized between the image of the cornea at the aligned location and images generated by placing the cornea at different locations.

At each cornea position, the beam was scanned in angle for the two-mirror system and transverse beam location for the one-mirror system. The power coupling coefficient between the illumination and scattered beam was calculated at each mirror position using equation (6) where E_i is the illumination beam and E_r is the scattered (reflected) beam.

$$\mathrm{K} = \frac{\left|\iint \overrightarrow{E_i} \cdot \overrightarrow{E_r}\, dA\right|^2}{\int \left|\overrightarrow{E_i}\right|^2 \mathrm{dA} \int \left|\overrightarrow{E_r}\right|^2 \mathrm{dA}} \tag{6}$$

The mirror positions were mapped to beam centroid locations on the cornea and an image was then generated by tabulating coupling coefficient and corresponding centroid position. Examples of the aligned case coupling coefficient maps are displayed in Figure 5a and b for the one mirror and two mirror systems respectively. Each image consists of 37 pixels, whose intensity is related to the power coupling coefficient. Parameters as OAP aperture and effective focal length limit the area that can be scanned, while the beam waist on the cornea limits the resolution of the image.

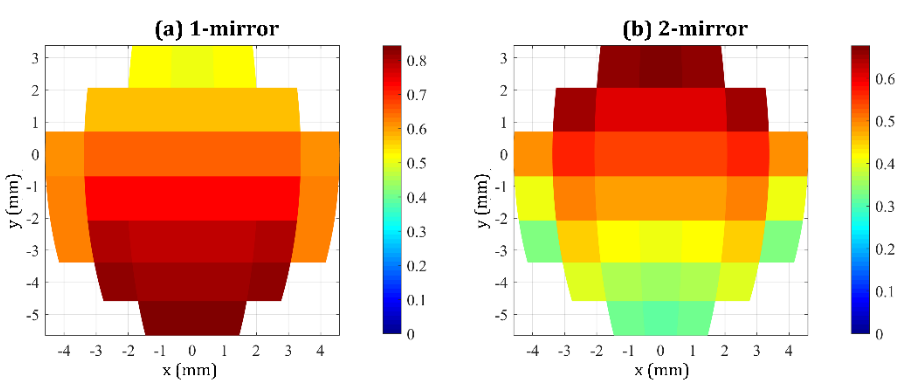

Figure 5: a) Coupling coefficient map on cornea the for the 1-mirror configuration. b) Coupling coefficients map on cornea for the 2-mirror configuration. The coupling coefficient has an opposite trend.

Once coupling coefficient maps were created for all 125 positions, the normalized cross-correlation coefficient was computed between the aligned case (x,y,z) = (0,0,0) and all other positions. This cross-correlation operation is described by (7) where μ_i and σ_i are the average and the standard deviation of the image i, respectively:

$$\rho_t = \frac{1}{n}\sum_{x,y}\frac{1}{\sigma_f\sigma_t}\left(f(x,y) - \mu_x\right)\left(t(x,y) - \mu_t\right) \tag{7}$$

Normalized cross correlation is a good candidate metric as it ignores the overall magnitude of each coupling coefficient map and focuses on spatial differences (patterns) between the aligned map f and the misaligned cases t:

6. RESULTS

6.1 1-mirror objective results

Our physical optics simulation results, displayed in Figure 5a, agree with the previously computed power coupling coefficients by Sung et al, which were obtained through ABCD quasioptics matrices and GRASP, a software package that implements Physical Optics[2].

As shown in Figure 6, most misalignments yield anticorrelated images except for a few positions. Interestingly, the cross-correlation is not only a function of the misalignment size but seems to also depend strongly on its direction. This configuration is very sensitive to misalignment, as a displacement of 0.5 mm produces an anticorrelated image in most cases. When the cross-correlation is positive, it is not because the sphere center of curvature is close to the focus, thus cross-correlation does not seem to provide any information on the location.

6.2 2-mirror objective results

The power coupling coefficient in the 2-mirror configuration results in an opposite trend than the 1 mirror case. The power coupling coefficient increases in the positive y-axis direction. The two systems are not comparable in terms of absolute values of the power coupling coefficients: as the beam radius on the cornea is a function of the beam waist radius located at the feed[2]. A plausible explanation for the coupling coefficient trend might be that the presence of the second mirror balances some cross-polarization effects and introduces further distortions for other locations [4, 5].

The cross-correlation pattern is not surprising: images generated with a smaller misalignment have also a higher correlation. The cross-correlation is at maximum 0.92 for misalignment of 0.5 mm, and 0.87 for misalignment of 1 mm. Also in this case the direction of the misalignment is important. The values suggest that it is possible to create a threshold of uncertainty that allows to quantify how misaligned the patients' eye is. It is likely, that these values can be further diminished/separated by the optical elements in front of the objective optics as the walk-off at least should start to amplify the errors introduced in the misaligned cases.

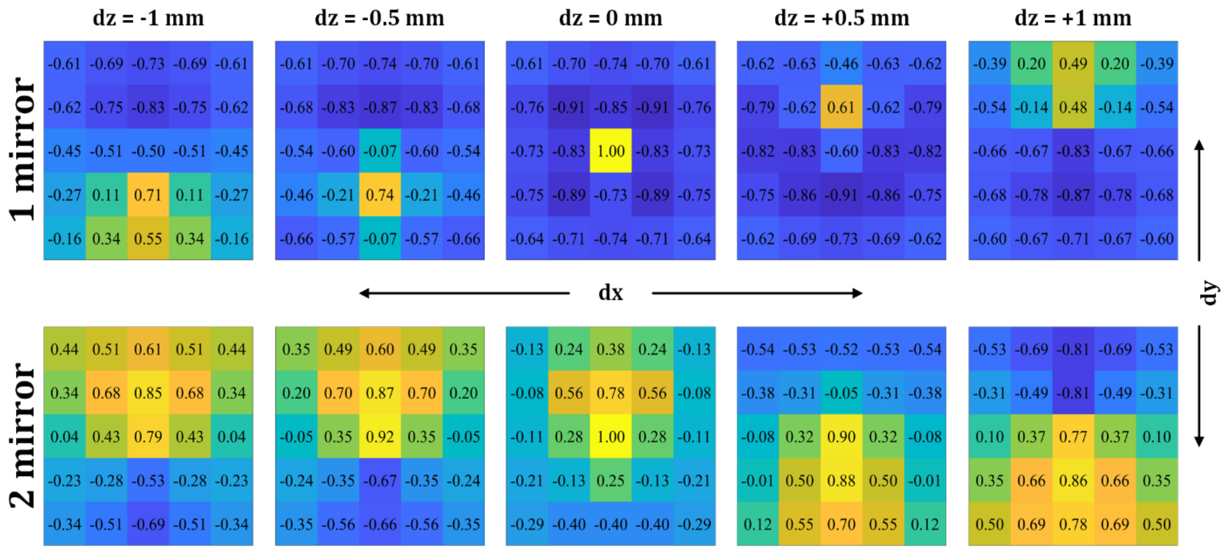

Figure 6: a) Misalignment cross-correlation for the 1-mirror and 2-mirror objectives

7. CONCLUSIONS

In this paper we illustrated two different configurations to implement a quasioptical SUBMMW system to measure the cornea water content and thickness. In particular, we analyzed two possible designs of an adjunct system, which would help in resolving misalignment errors. In the 2-mirror system case, normalized cross-correlation of images is associated with misalignment magnitude. We studied only the final optic behavior, so it is important to stress that the rest of the system could be designed to make the optics more sensitive to misalignment. We believe that one configuration, the 2-mirror objective, is simpler to realize than the other, the 1-mirror one, because it is easier to implement a faster and more precise scanning by rotating a mirror than mechanically translating two of them.

Physical Optics is an appropriate simulation technique for millimeter and submillimeter waves, but it is computationally heavy. Therefore, ray-tracing methods could be used for design as they yield sufficiently accurate results under certain conditions[6].

It was shown that a contained misalignment produces variations that are non-obvious functions of the cornea position. Other parameters such as average coupling coefficient and coupling coefficient variance could be included in the analysis and machine learning could be used to train the system to estimate the misalignment.

ACKNOWLEDGMENTS

The calculations presented above were performed using computer resources within the Aalto University School of Science “Science-IT” project.

REFERENCES

[1] Vinh, N. Q., Sherwin, M. S., Allen, S. J., George, D. K., Rahmani, A. J. and Plaxco, K. W. , "High-precision gigahertz-to-terahertz spectroscopy of aqueous salt solutions as a probe of the femtosecond-to-picosecond dynamics of liquid water," J.Chem.Phys. 142(16), 164502 (2015).

[2] Sung, S., Dabironezare, S., Llombart, N., Selvin, S., Bajwa, N., Chantra, S., Nowroozi, B., Garritano, J., Goell, J., Li, A., Deng, S. X., Brown, E. R., Grundfest, W. S. and Taylor, Z. D. , "Optical System Design for Noncontact, Normal Incidence, THz Imaging of in vivo Human Cornea," IEEE Transactions on Terahertz Science and Technology 8(1), 1-12 (2018).

[3] Taylor, Z., Garritano, J., Sung, S., Bajwa, N., Bennett, D. B., Nowroozi, B., Tewari, P., Sayre, J., Hubschman, J., Deng, S., Brown, E. R. and Grundfest, W. S. , "THz and mm-Wave Sensing of Corneal Tissue Water Content: Electromagnetic Modeling and Analysis," IEEE Transactions on Terahertz Science and Technology 5(2), 170-183 (2015).

[4] Goldsmith, P. F. , "Practical Aspects of Quasioptical Focusing Elements," Quasioptical Systems: Gaussian Beam Quasioptical Propogation and Applications, 69-124 (1998).

[5] Brückner, C., Notni, G. and Tünnermann, A. , "Optimal arrangement of 90° off-axis parabolic mirrors in THz setups," Optik 121(1), 113-119 (2010).

[6] O'Sullivan, C., Atad-Ettedgui, E., Duncan, W., Henry, D., Jellema, W., Murphy, J. A., Trappe, N., van de Stadt, H., Withington, S. and Yassin, G. , "Far-Infrared Optics Design & Verification," Int J Infrared Millim Waves 23(7), 1029-1045 (2002).